A Comparative Study of Point Processes for Line Network Extraction in Remote Sensing

Caroline Lacoste, Xavier Descombes, Josiane Zerubia

INRIA

INSTITUT NATIONAL DE RECHERCHE EN INFORMATIQUE ET EN AUTOMATIQUE

A Comparative Study of Point Processes for Line Network Extraction in Remote Sensing

Caroline Lacoste — Xavier Descombes — Josiane Zerubia

N° 4516

Juillet 2002

THÈME 3

ISSN 0249-6399 ISRN INRIA/RR--4516--FR+ENG

INRIA
SOPHIA ANTIPOLIS

A Comparative Study of Point Processes for Line Network Extraction in Remote Sensing

Caroline Lacoste , Xavier Descombes , Josiane Zerubia

Thème 3 — Interaction homme-machine,
images, données, connaissances
Projet Ariana

Rapport de recherche n° 4516 — Juillet 2002 — 53 pages

Abstract: We present in this report a comparative study between models of line network extraction, within a stochastic geometry framework. We rely on the theory of marked point processes specified by a density with respect to the uniform Poisson process. We aim to determine which prior density is the most relevant for road network detection. The "Candy" model, introduced in [21] for the extraction of road networks, is used as a reference model. This model is based on the idea that a road network can be thought of as a realization of a Markov object process, where the objects correspond to interacting line segments. We have developed two variants of this model which use quality coefficients for interactions. The first of these two variants is a generalization of the "Candy" model and the second one is an adaptation of the "IDQ" model proposed in [13] for the problem of building extraction from digital elevation models. The optimization is achieved by a simulated annealing with a RJMCMC algorithm. The experimental results, obtained for each model on aerial or satellite images, show the interest of adding quality coefficients for interactions in the prior density.

Key-words: Point processes, RJMCMC, line network extraction.

Unité de recherche INRIA Sophia Antipolis
2004, route des Lucioles, BP 93, 06902 Sophia Antipolis Cedex (France)
Téléphone : +33 4 92 38 77 77 —Télécopie : +33 4 92 38 77 65

Etude Comparative de Processus Ponctuels pour l'Extraction de Réseaux Linéiques en télédétection

Résumé : Nous présentons, dans ce rapport, une étude comparative entre plusieurs modèles d'extraction de réseaux linéiques, issus de la géométrie stochastique. Nous nous plaçons dans le cadre des processus ponctuels marqués spécifiés par une densité par rapport au processus de Poisson homogène. L'objectif de cette étude est de déterminer quelle type de densité *a priori* est la plus adaptée à cette probématique de détection de réseaux linéiques, et plus particulièrement de réseaux routiers. Nous reprenons le "Candy" modèle, introduit dans [21] pour l'extraction de réseaux routiers, et nous l'utilisons comme modèle de référence. Ce modèle est basé sur l'idée qu'un réseau routier peut être assimilé à une réalisation d'un processus Markov objet, où les objets correspondent à des segments en interaction. Nous proposons deux variantes de ce modèle qui font intervenir des coefficients mesurant la qualité des interactions entre objets. La première est une généralisation du "Candy" modèle et la seconde correspond à une adaptation du modèle "IDQ", proposé dans [13] pour l'extraction de bâtiments dans les modèles numériques d'élévation. Nous réalisons l'optimisation de chaque modèle par un recuit simulé sur un algorithme MCMC à sauts réversibles. Les résultats expérimentaux obtenus pour les trois modèles, sur des images satellitaires ou aériennes, permettent de vérifier l'intérêt de l'intégration de la qualité des interactions dans la densité *a priori*.

Mots-clés : Processus ponctuels, RJMCMC, extraction de réseaux linéiques.

Contents

1 Introduction

In the perspective of cartographic update assistance, we aim to extract road networks from images. Motivated by the increase of data acquisition, a wide variety of methods have been - and will be - developed in order to answer to this difficult problem. A first possibility is provided by semi-automatic approaches where an operator gives starting points and directions in order to initialize a following road algorithm, as for instance in [4], or some checking points which may be linked by an algorithm based on dynamic programming, as in [10], or on deformable contour models, as in [12]. This methods can be extended to fully-automatic ones by an automatic detection of road seeds [2, 24]. A multi-scale approach is also used to combine detection of the road central line at coarse level and road borders at fine level [9]. Another way to automatically provide a result is the use of combined low-level operators [3]. A non-supervised technique, which is not based on a combination of several processings on the image - as for the previous fully-automatic techniques - , is modeling road networks by a Markov object process. Indeed, these recently developed models allow us to use stochastic properties as those of Markov fields while using strong geometrical constraints. Moreover, it avoids the important sensitivity to noise and local minima of the usual pixel approaches.

The line network S is seen as realization of a Markov object process $\mathbf{S}$ where the objects are interacting segments. Such a process can be specified by a density f with respect to the distribution of a uniform Poisson point process which is a completely random (marked) point process. It is the case of the "Candy" model defined in [21] for line network extraction from aerial and satellite images.

In order to achieve the detection of objects from images, this density has to be composed by two different terms. First, a prior knowledge has to be integrated into the density in order to smooth the solution and avoid breaks in the line network. Second, a data term is used to fit the data. Thus, the density of the point process can be written as the product of a prior density h_p and a data term h_d :

$$\boxed{f(S) \propto h_d(D/S)\ h_p(S)} \tag{1}$$

where S is a realization of $\mathbf{S}$ and D the pixel value grid of the considered image.

In this work, we have been interested in the construction of a good prior density in order to obtain a realistic line network. The performances of the "Candy" model

in simulating and detecting line network have already been shown. Moreover, its good stability and Markov properties have been proved in [23], which makes it a good reference model for line network extraction. In this report, two extensions of the "Candy" model are proposed and compared to this original model.

Each of those prior densities is defined in Section 2. To make a reliable comparison between each prior model, we use the same data term - defined in Section 3 - for the three models. Section 4 explains how the models can be sampled and how to optimize their densities with respect to the Poisson measure. Finally, some results are given in Section 5 leading to a comparative analysis of the three prior models.

2 Definition of the prior models

2.1 "Candy" model

This model is based on three types of possible relations between segments : the connection R_c and two relations of bad orientation, R_{io} (internal bad orientation) and R_{eo} (external bad orientation).

Two segments are said to be connected if two of their extremities are closer than a constant ϵ[1]. This relation (connection) defines several types of segments as shown in Figure 1. Free segments are those which are not connected ; single ones are those

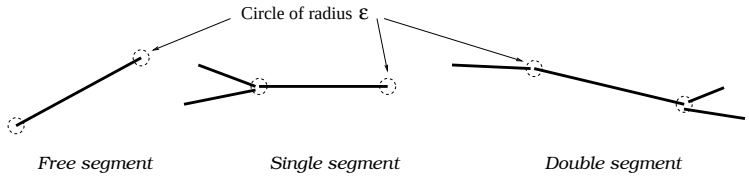

Figure 1: Segment types defined with respect to R_c.

with only one of their endpoints connected to other segments ; and double segments have their two endpoints connected. In the density, the first two types of segments (free and single) are penalized in order to avoid breaks in the network and false alarms, the assumption being that most roads are not so short that can be described

[1]Note that, under the Poisson process, no exact connection between pair of segments occurs almost surely.

by a free segment.

In order to avoid superposition of line segments or pairs of segments crossing at too sharp angle while allowing crossing at right angle, the internal bad orientation, R_{io}, is defined. Pairs of segments in internal bad orientation are penalized. It con-

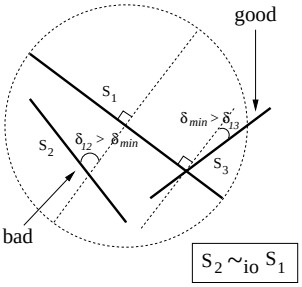

Figure 2: Internal bad orientation R_{io}.

cerns segments whose midpoints and orientations are too close[2]. So, in Figure 2, the pair (s_1, s_2) is concerned by this relation (R_{io}) and (s_1, s_3) is not.

The last relation R_{eo} has been introduced to control the curvature of the line network. Thus, R_{eo} concerns pairs of segments whose midpoints are located further than the larger radius of these segments and whose two extremities are close enough. In this case, if they are disoriented, like s_1 and s_3 in Figure 3, they are said to be in external bad orientation.

The pairwise interaction potential of the "Candy" model is a weighted sum of the numbers of free segments n_f, of single segments n_s and of bad pairs of segments with respect to R_{io} and R_{eo}. So, the prior density of the "Candy" model can be written as follows :

$$\boxed{h_p(S) \propto \beta^n \exp\left[-\omega_f n_f - \omega_s n_s - \omega_{io} n_{io} - \omega_{eo} n_{eo}\right]} \tag{2}$$

[2]For more precision, see [21, 23].

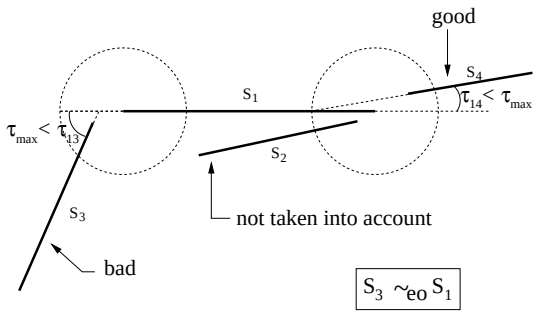

Figure 3: External bad orientation R_{eo}.

where :
$$\begin{cases} n & : \text{total number of segments,} \\ n_f & : \text{number of free segments,} \\ n_s & : \text{number of single segments,} \\ n_{io} & : \text{number of pairs of segments corresponding to } R_{io}, \\ n_{eo} & : \text{number of pairs of segments corresponding to } R_{eo}, \\ \omega_i & : \text{positive weights,} \\ \beta & : \text{intensity factor.} \end{cases}$$

This density specifies a well-defined marked point process, as the Ruelle 's stability condition [19] is verified. This condition and the stronger condition of local stability are proven in [23]. Moreover, the "Candy" model is a Markov process with respect to the relation $\sim$ defined by :

$$s \sim s' \Longleftrightarrow d(p_s - p_{s'}) \leq 2(L_{max} + \epsilon)$$

where p_s denotes the midpoint of the segment s, and d the Euclidean distance in R^2. This property allows to reduce the cost of one iteration in the $RJMCMC$ algorithm defined in Section 4.

Nevertheless, the density takes the same value for configurations which do not have the same quality, as we can see in Figure 4. Thus, we can obtain a line network with little breaks between connected extremities and not as smooth as possible. That is the reason why we have introduced quality coefficients to smooth the solution in the two following models.

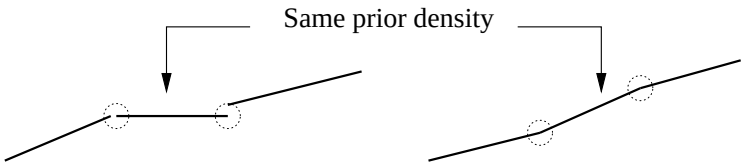

Figure 4: A drawback of the "Candy" model.

2.2 "Quality Candy" model

Considering the "Candy" model as a good starting point, we have chosen to keep its general structure, only replacing constant potential of interaction by variable functions g_r for different relations between segments. The prior density is now given by the following formula :

$$\boxed{h_p(S) \propto \beta^n \exp\left[-n_f\omega_f - n_s\omega_s - \sum_{r\in\mathcal{R}} \omega_r \sum_{<s_i,s_j>_r} g_r(s_i,s_j)\right]} \tag{3}$$

where : $\begin{cases} n, n_f, n_s \text{ are defined as before,} \\ <,>_r \text{ denotes a pair of interacting segments with respect to } r, \\ g_r(.,.) \equiv \text{potential function with respect to } r. \end{cases}$

One can notice that if we take the 2 relations of bad orientation of the first model and a potential function equal to 1 in any case, we get back to the "Candy" model. Thus, this model can be seen as a generalization of the "Candy" model.

First of all, we have chosen to redefine the relation of connection adding a constraint to accelerate the optimization algorithm. From now on, two segments are said to be connected if the angle they form is not sharp. For example, in Figure 5, s_1 and s_3 are not connected. Moreover, in order to promote pairs of segments whose endpoints and orientations are close, like (s_1, s_2) in Figure 5, a potential function g_{R_c} is defined for pairs of connected segments as the mean of two functions :

$$\text{for } s_i \sim_c s_j \ , \ g_{R_c}(s_i,s_j) = \frac{g_\tau(\tau_{ij}) + g_\epsilon(d_{ij})}{2} \tag{4}$$

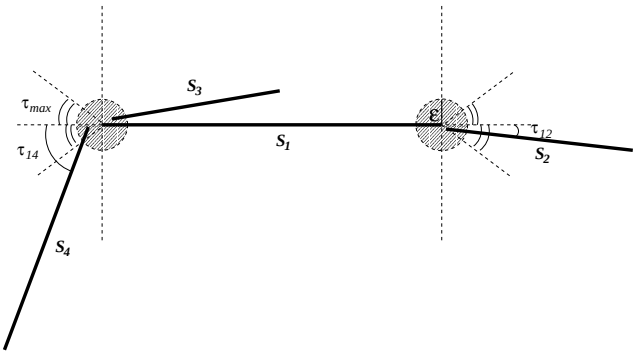

Figure 5: Different types of connection - (s_1,s_2) : attractive connection - (s_1,s_3) : not considered as a connection - (s_1,s_4) : repulsive connection with respect to the orientation.

$$\text{with} \begin{cases} g_\tau(\tau_{ij}) = \begin{cases} -\sigma(\tau_{ij}, \tau_{max}) \text{ if } |\tau_{ij}| < \tau_{max} \\ 1 \text{ if not} \end{cases} \\ g_\epsilon(d_{ij}) = -\sigma(d_{ij}, \epsilon) \end{cases}$$

Here, g_τ deals with orientation. It gives an attractive ($\equiv$ negative) weight to pairs of segments (s_i, s_j) whose difference of orientation τ_{ij} is lower than a threshold τ, and a repulsive ($\equiv$ positive) one in the other case. Whereas g_ϵ deals with the difference d_{ij} between extremities and is attractive.

The attractive terms of these two functions are given by the quality function σ given in equation (5) :

$$\begin{array}{rccl} \sigma(.,M): & [-M,M] & \longrightarrow & [0,1] \\ & x & \longmapsto & \sigma(x,M) = \dfrac{1}{M^2}\left(\dfrac{1+M^2}{1+x^2} - 1\right) \end{array} \tag{5}$$

This is a positive function for values in $[-M, M]$, which takes its maximum for a difference of orientation or a distance equal to 0, as shown in Figure 6.

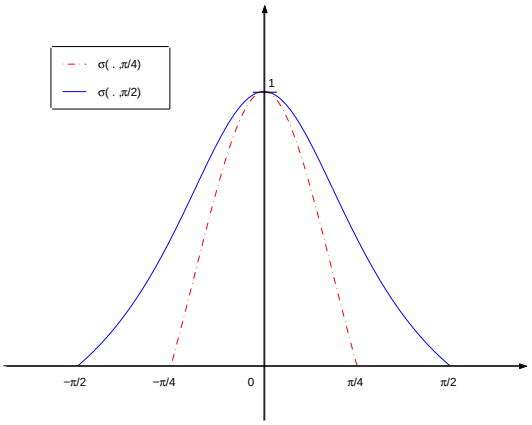

Figure 6: Quality function for two maximal boundary : $M = \pi/2$ and $M = \pi/4$.

Moreover, this new potential allows us to work without the relation of external bad orientation R_{eo}, as the repulsive part of the connection potential concerns the same type of interaction.

Finally, we keep exactly the same relation for internal bad orientation, but redefine the potential function. Pairs of segments forming a too sharp angle are forbidden for stability reasons. So, an infinite weight is given to them (i.e. "hard-core" potential). For the other pairs in internal bad orientation, we use the same quality function σ to define a repulsive weight based on the difference of orientation between the two segments. So, for each pair (s_i, s_j) such that $s_i \sim_{io} s_j$, the formula is the following :

$$g_{R_{io}}(s_i, s_j) = \begin{cases} \infty \text{ if } \tau_{ij} < c \\ 1 - \sigma(\tau_{ij}, \pi/2 - \delta_{min}) \end{cases} \quad (6)$$

where τ_{ij} is the difference of orientation between s_i and s_j , and δ_{min} is the minimal difference with respect to the right angle from which two segments are considered as disoriented, and c the minimal difference of orientation which can be present in the configuration.

To sum up, the "Quality Candy" model only holds on two relations between segments : the connection which can be an attractive or a repulsive interaction, and the

internal bad orientation, which is always repulsive. Moreover, this model is locally stable as proven hereafter which guarantees the ergodic convergence of the algorithm described in Section 4.

Stability proof

To prove the local stability (stronger condition than Ruelle's one), a superior bound for the ratio $\frac{h_p(S\cup s')}{h_p(S)}$*, for all* S *in* $\Omega = \bigcup_{i=1}^{\infty}\{S \subset F/\ n(S) = i\}$ *and* s' *in* $U = [F \times K]$ *(where* $F \subset \mathbb{R}^2$ *is the compact set where points - segment midpoints - are observed, and* K *the mark space - space of lengths and orientations -) has to be found whenever* $h_p(S) > 0$*.*

The expression of $\frac{h_p(S\cup s')}{h_p(S)}$ *is the following :*

$$\frac{h_p(S\cup s')}{h_p(S)} = \beta \exp \quad [-\omega_f \underbrace{(n_f(S\cup s') - n_f(S))}_{A} - \omega_s \underbrace{(n_s(S\cup s') - n_s(S))}_{B} - \omega_c \underbrace{\sum_{<s_i,s'>_c} g_{R_c}(s_i,s')}_{C} - \omega_{io} \underbrace{\sum_{<s_i,s'>_{io}} g_{R_{io}}(s_i,s')}_{D}\ ] \tag{7}$$

Thus, uniformly bounding from below the parts A*,* B C *and* D*, is sufficient to prove local stability.*

Firstly, considering the term A *of equation (7) , the addition of a segment* s' *in the configuration* S *gives :*

$$n_f(S\cup s') - n_f(S) = \begin{cases} 1 \text{ if } s' \text{ is free} \\ -\sharp(\{\ s_i \text{ free in } S/s' \sim_c s_i\ \}) \text{ if } s' \text{ is single or double} \end{cases}$$

where $\sharp(.)$ *denotes the cardinal of a set. Here, the number of free segments in* S *which may be connected to a new segment* s' *cannot be bounded as it has been done for the "Candy" model*[3]*. Indeed, an infinity of segments could be within a ball of radius* ϵ *without being connected, as two segments forming a sharp angle are not connected. This is the reason why a "hard-core" potential has been introduced for*

[3]If R_c is defined for every difference of orientation, as in the "Candy" model, the maximal number of free segments for which an endpoint is within a ball of radius ϵ is 6.

pairs of segments forming a too sharp angle (see equation (6)). Pairs of segments in internal bad orientation - which is the case of non connected segments whose two extremities are at a distance smaller than ϵ because they form a sharp angle - are not present in the compact set $F \in \mathbb{R}^2$ almost surely, if the difference of orientation between the two segments forming the pair is lower than a constant c : in this case , $h_p(S) = 0$. So, such configurations must not be taken into account in the stability study. Consequently, the number of segments connected to one endpoint of s' is bounded by n_{max}, the maximal number of segments for which one endpoint is on the same ball of radius ϵ, with a minimal difference of orientation of c and a maximal difference of orientation equal to π (as a connection only occurs when the formed angle is larger than $\pi/2$). So, n_{max} is given by :

$$n_{max} = E(\frac{\pi}{c}) + 1$$

where c is expressed in radian and E denotes the integer part. The minimal bound of A is obtained for the case of a birth of a double segment s', connected to n_{max} segments at each of its endpoints :

$$A > -2\, n_{max}$$

Secondly, B can be decomposed as follows :

$$n_s(S \cup s') - n_s(S) = \begin{cases} 1 \text{ if } s' \text{ is free} \\ \\ 1 + \sharp(\{\, s_i \text{ free in } S/s' \sim_c s_i \,\}) \\ -\sharp(\{\, s_i \text{ single in } S\} \cap \{s_i \text{ double in } (S \cup s')\,\}) \text{ if } s' \text{ is single} \\ \\ \sharp(\{\, s_i \text{ free in } S/s' \sim_c s_i \,\}) \\ -\sharp(\{\, s_i \text{ single in } S\} \cap \{s_i \text{ double in } (S \cup s')\,\}) \text{ if } s' \text{ is double} \end{cases}$$

The worst case occurs when a maximal number of single segments in S becomes double segments in $(S \cup s')$. Thus,

$$B > -2\, n_{max}$$

Thirdly, given equation (4) and the fact that the quality function is bounded from above by 1, $g_{R_c}(s_i, s_j) > -1$. Thus, the sum C is bounded as follows :

$$C > -2\, n_{max}$$

Then, as $g_{R_{io}}(s_i, s')_d$ is a positive function, the expression D is bounded from below by 0.

$$D > 0$$

Finally, $\forall s'$ *and* $\forall S \in \Omega / f(S) \neq 0$,

$$\boxed{\frac{h_p(S \cup s')}{h_p(S)} < \beta \, \exp\left[2 \, (\omega_f + \omega_s + \omega_c) \, \left(E(\frac{\pi}{c}) + 1\right)\right]} \tag{8}$$

which proves that the "Quality Candy" model is locally stable.

2.3 "IDQ" model

This subsection briefly presents the "IDQ" model introduced in [13] in order to extract buildings from digital elevation models. For each relation r, cliques with respect to r that are formed by a given number of objects c_r (for example, $c_r = 2$ for pairwise interactions) are considered. To simplify, we call them c_r-cliques. The relations taking part in the model are described by three global terms on the configuration of objects S :

- the **intensity** I which is defined as the average of numbers of c_r-cliques to which an object belongs. Here is its expression :

$$I(r, S) = \frac{c_r \, N_c(r, S)}{N_o(r, S)} \tag{9}$$

  where $N_c(r, S)$ is the number of c_r-cliques and $N_o(r, S)$ the number of objects concerned by r in S.

- the **diffusion** D which is the proportion of segments in a c_r-clique. It is given by :

$$D(r, S) = \frac{N_o(r, S)}{n(S)} \tag{10}$$

  where $n(S)$ is the total number of objects in S.

- the **quality** Q defined as the mean of a quality function - defined as in Section 2.2 - on each c_r-clique. For instance, for pairwise interaction :

$$Q(r, S) = \frac{1}{N_c(r, S)} \sum_{<s_i, s_j>_r} \sigma_r(s_i, s_j) \tag{11}$$

where $\sigma_r(s_i, s_j)$ denotes the value of the quality function for a pair of interacting segments with respect to r, $< s_i, s_j >_r$.

The prior density is then the product of three interaction functions f_I, f_D and f_Q respectively depending on I, D and Q.

$$\boxed{h_p(S) \propto \beta^n \prod_{R \in \mathcal{R}} f_I(R) f_D(R) f_Q(R)} \tag{12}$$

where the interaction functions f_y can be written as follows :

- For $y = I$ or $y = D$: $f_y(R) = \exp\left[-\gamma_{y,R} \left(y(R) - y_o\right) \log\left(\frac{y(R) + \eta}{y_o + \eta}\right)\right]$
  where y_o is the optimal value chosen for $y = I$ or D, and η a small constant.

- For Q : $f_Q(R) = \exp\left[-\gamma_{Q,R} \left(Q(R) - 1\right)\right]$.

These interaction functions have good properties : they exhibit an exponential form with a convex potential reaching its minimum for a chosen optimal value. Moreover, the logarithmic potential for D and Q lead to work with quantities of the same order as the factor of intensity β. The "IDQ" density specifies a well-defined point process which is locally stable [13].

In our case, objects are pairwise interacting segments and we consider the same relations as for the "Quality Candy" model. For the connection R_c, we have chosen $I_o = 2$ for intensity because we want segments to be doubly connected in mean, and $D_o = 1$ for diffusion because free segments have to be avoided. For the relation of bad orientation R_{io}, only the diffusion is taken into account with an optimal value D_o set to 0.

3 Data modeling

In order to extract line networks from any image, we need a realistic and robust modeling of the data. This section describes the construction of the data term.

Given a configuration of segments, S, the subsets of pixel values corresponding to each segment and its neighborhood are supposed to be independent. This simplifying

hypothesis allows a factorization of the data term. Within a Gibbs framework, the general form of the data term is thus given by :

$$h_d(D/S) \propto \exp\left[-\gamma_d \sum_{s_i \in S} \delta_i\right] \tag{13}$$

where δ_i is some statistical value (defined below) computed on the set of pixel values corresponding to a region defined as the neighborhood of the segment s_i on the image D. γ_d is a positive and constant weight.

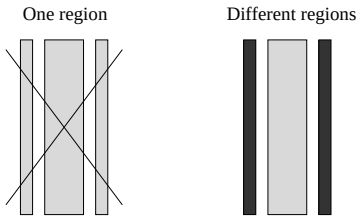

Figure 7: H_1 - Significant difference with the near background.

The potential δ_i is based on two hypothesis with respect to a line segment and its neighborhood. We first suppose that the background regions are different, at least on average, from the segment region (see Figure 7). Secondly, the set of pixel

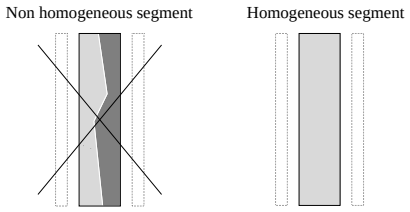

Figure 8: H_2 - Segment homogeneity.

values corresponding to a segment has to be homogeneous, otherwise edges could be detected instead of roads (see Figure 8).

To check these hypotheses for a given segment s_i, this segment is divided into several regions b_1, ..., b_n. Moreover, two strips on both sides of a segment s_i, R_1^i

and R_2^i, are considered, at a distance d from the segment in order to allow a range of widths. This is illustrated in Figure 9. Considering pixel values of each strip as a

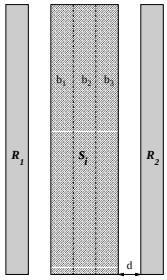

Figure 9: Division of segment into several strips.

sample of a population, a Student's t-test is used to determine if the averages of the two samples are significantly different. This statistical test deals with the problems associated with inference based on small samples which is our case, especially when a segment is near the boundary of the image. The formula for the t-test is a ratio. The top part of the ratio is the difference between the two sample means. The bottom part is a measure of the variability of the sample. Here is the t-test expression for two samples x and y :

$$\text{t-test}(x,y) = \frac{|\overline{x} - \overline{y}|}{\sqrt{\frac{\widetilde{\sigma}_x}{n_x} - \frac{\widetilde{\sigma}_y}{n_y}}} \tag{14}$$

where $\overline{x}$, $\widetilde{\sigma}$ and n respectively refer to the sample mean, the sample standard deviation, and the number of observations.

Above some critical value, we can consider that these two samples come from two populations of different means. Thus, the statistical value for mean difference hypothesis H_1 is the minimum of the test value between the whole segment and a border region :

$$T_{H_1}(s_i) = \min_{l \in \{1,2\}} \left[\text{t-test}(R_l^i, s_i) \right]$$

and the statistical value for homogeneity hypothesis H_2 is the maximal t-test between two inside regions :

$$T_{H_2}(s_i) = \max_{j,k \in \{1,..,n_b\}, j \neq k} \left[\text{t-test}(b_j, b_k) \right]$$

Then, the potential value for each segment is the ratio of this two quantities, with the additional condition that $T_{H_2}(s_i)$ is lower than 1 in order to forbid division by infinity and avoid promoting excessively very homogeneous regions.

$$T_i = \frac{T_{H_1}(s_i)}{\max\left[\,1\,,\,T_{H_2}(s_i)\,\right]} \tag{15}$$

Moreover, we proceed to a thresholding and a conversion of the test values from $[0,\infty]$ to $[-1,1]$. Finally, the potential value is the following :

$$\delta_i = \begin{cases} 1 & \text{if } T_i < t_1 \\ 1 - 2\,\frac{T_i - t_1}{t_2 - t_1} & \text{if } t_1 < T_i < t_2 \\ -1 & \text{if } T_i > t_2 \end{cases} \tag{16}$$

where t_1 and t_2 $(t_1 < t_2)$ are two empirically chosen positive thresholds.

This potential δ_i associated to the segment s_i is a dual potential : it can take attractive (negative) values, and repulsive (positive) values. Thresholds t_1 and t_2 are robust in the sense that results are similar if we modify a little bit their values, and that we can use the same thresholds for two different images provided that the two line networks are similar enough (i.e. nearly the same contrast between roads and the background, nearly the same homogeneity).

To verify the relevance of this potential function, we have computed its mean value in each pixel of the image grid. More precisely, we have computed the mean values for segments of minimal length L_{min}, whose midpoint is on the considered pixel, for 24 orientation in $[-\pi,\pi]$. Figure 10 gives an example on a SPOT image. The negative values of the potential δ_i are in white - the pixel is then a good choice for a segment center - and the positive values of δ_i are in black. This result confirms that the proposed data term choice is reasonable.

To summarize, we have constructed a data term with an exponential form whose the energy can be easily computed. Moreover, it is based on statistical tests which seem to be adapted to line network recognition.

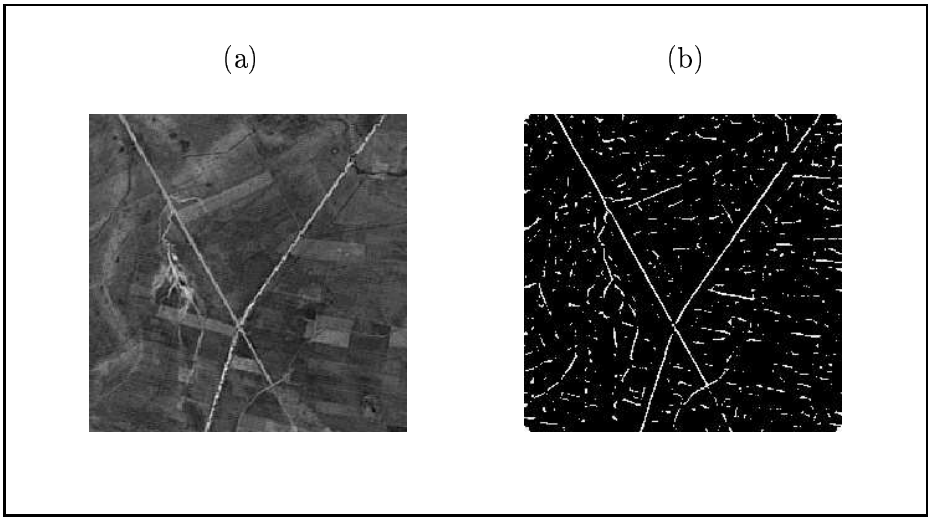

Figure 10: Data term on a spot image - (a) : data - (b) : sign of the mean value of the potential, computed for a fixed segment length and 24 segment orientations.

4 Reversible Jump Monte Carlo Markov Chain algorithm

4.1 Simulation of spatial point processes

Let's recall that the distribution of the point process π is supported by a state space of varying dimension. The state space is :

$$\Omega = \bigcup_{i=1}^{\infty} \Omega_i \quad \text{with } \Omega_i = \{S \subset F / \ n(S) = i\}$$

where $F \subset \mathbb{R}^2$ is the compact subset corresponding to the image.

To deal with this probability measure in which the random variable has a randomly variable dimension, two types of algorithms have been proposed in the literature : Birth and Death (BD) samplers, based on a spatial birth and death process [14, 16], and Reversible Jump Monte Carlo Markov Chain (RJMCMC) algorithms [5, 6], where the generated Markov chain S_t performs small jumps between the spaces Ω_i. Two main reasons have prompted us to use a RJMCMC algorithm to simulate the models defined in the previous section. Firstly, in many cases, the BD sampler

is less efficient, as it has been shown in [8]. Secondly, the BD algorithm only allows birth or death of an object, whereas several types of updates - such as translation, rotation, dilation of an object - can be defined in the RJMCMC algorithm. So, if relevant moves are proposed, the algorithm convergence is faster, especially when the process is geometrically constrained.

The RJMCMC algorithm consists in simulating a discrete Markov Chain with a Metropolis-Hastings-Green dynamics [5, 6]. The measure of interest occurs as the stationary measure of the chain. This iterative algorithm does not depend on the initial state. Table 1 describes one iteration of the algorithm. At each step,

At step t, $S_t = S$:
1. Sample $S' \sim Q(S \rightarrow .)$
2. Evaluate Green's ratio $R(S, S')$
3. Move to the state S' with probability $\alpha(S, S') = \min(1, R(S, S'))$

Table 1: RJMCMC algorithm.

a transition from the current state S to a new state S' is proposed according to a proposition kernel $Q(S \rightarrow .)$. The transition is accepted with a probability $\alpha(S, S')$ given by the Green's ratio. This acceptance ratio is computed so that the detailed balance condition is verified, condition under which this algorithm converges to the unnormalized measure of the spatial point process π. The expression of this strong condition is given by the equation (17) :

$$\int_A \int_B \pi(dS)\, P(S, dS') = \int_B \int_A \pi(dS')\, P(S', dS) \tag{17}$$

where A and B are two Borel subsets of Ω, π is the measure of the spatial point process, and $P(,)$ the transition kernel of the Markov chain S_t, defined as follows :

$$\begin{aligned} P(S,A) &= P(S_{t+1} \in A | S_t = S) \\ &= \underbrace{\int_A \alpha(S,S') Q(S \to dS')}_{\text{acceptance case}} + \underbrace{\mathbf{1}[S \in B] \int_\Omega (1 - \alpha(S,S')) Q(S \to dS')}_{\text{rejection case}} \end{aligned} \tag{18}$$

where $\mathbf{1}[.]$ denotes the indicator function.

To hold condition (17), it is sufficient that :

$$\int_A \pi(dS) \int_B Q(S \to dS')\, \alpha(S,S') = \int_B \pi(dS') \int_A Q(S' \to dS)\, \alpha(S',S) \quad \forall A, B \subset \Omega \tag{19}$$

Furthermore, supposing that $\pi(dS)\, Q(S \to dS')$ has a finite density, $\mathcal{D}^{\pi Q}$, with respect to a symmetrical measure ψ on $\Omega \times \Omega$, the condition (17) can be written as follows :

$$\alpha(S,S')\, \mathcal{D}^{\pi Q}(S,S') = \alpha(S',S)\, \mathcal{D}^{\pi Q}(S,S') \tag{20}$$

Finally, taking the choice made in [11] :

$$\alpha(S,S') = \min\left\{1, R(S,S')\right\} \tag{21}$$

where R is the Green's ratio given by :

$$R(S,S') = \frac{\mathcal{D}^{\pi Q}(S',S)}{\mathcal{D}^{\pi Q}(S,S')} \tag{22}$$

equality (20) is verified.

One interesting point of the Metropolis-Hastings-Green algorithm is that the proposition kernel Q can be decomposed into several kernels q_i, each corresponding to a reversible move, as it has been proposed in [6]. The algorithm is the same as in Table 1, replacing Q by a randomly chosen kernel q_i. The procedure is given in Table 2. In the next section, several transition kernels are proposed and the explicit formula of the associated Green's ratio is given.

At step t, $S_t = S$:

1. Randomly choose a type of move i
2. Sample $S' \sim q_i(S \to .)$
3. Evaluate $R_i(S, S') = \dfrac{\mathcal{D}^{\pi q_i}(S', S)}{\mathcal{D}^{\pi q_i}(S, S')}$
4. Move to the state S' with probability $\alpha = \min(1, R_i(S, S'))$

Table 2: RJMCMC algorithm with several moves.

4.2 Proposition kernel and computing Green's ratio

Although it is sufficient to define the uniform birth-and-death [5] - see Section 4.2.1 - in order to simulate a marked point process (theoretically, S_t should converge to the same measure), it is important to define more or less complex moves in order to accelerate the convergence of the Markov chain. For example, a simple move, such as a translation or a rotation, is more efficient than a death followed by a birth, leading to the same result. Such types of moves are described in Section 4.2.2. Furthermore, a birth-and-death within a neighborhood is often judicious, especially if objects are supposed to be in interaction. In Section 4.2.3, such a kernel with respect to the connection is defined and Green's ratio computation is presented in detail.

4.2.1 Uniform birth-and-death

The uniform birth-and-death is the simplest proposition kernel which allows to make small jumps between spaces of different sizes. It consists in a uniform birth in the compact set $F \subset \mathbb{R}^2$ - proposed with a probability p_b - and in a uniform death (inverse proposition) in the set of segments S. It is given by :

$$Q(S \to A) = p_b \, Q_b(S \to A) \; + \; p_d \, Q_d(S \to A) \tag{23}$$

where p_b (resp. $p_d = 1 - p_b$) is the probability of choosing a birth (resp. a death). The two parts of the kernel (Q_b and Q_d) respectively correspond to parts 2 and 3 of

At step t, $S_t = S$.

1. Choose a birth within a neighborhood with a probability p_b.
In this case go to 2, otherwise go to 3.

2. Birth case :

- $s' = [p, L, \theta]$ is uniformely drawed in $[\, F \times [L_{min}, L_{max}] \times [0, \pi] \,]$

- compute $R(S, S \cup s') = \dfrac{f(S \cup s')\, p_d\, (L_{max} - L_{min})\, \pi}{f(S)\, p_b\, (n(S) + 1)}$

- move to the state $S' = S \cup s'$ with probability $\alpha = \min(1, R(S, S \cup s'))$

3. Death case :

- choose $s' \sim \mathcal{U}\{\, S\}$

- compute $R(S, S \setminus s') = \dfrac{f(S \setminus s')\, p_b\, n(S)}{f(S)\, p_d\, (L_{max} - L_{min})\, \pi}$

- move to the state $S' = S \setminus s'$ with probability $\alpha = \min(1, R(S, S \setminus s'))$

Table 3: Uniform birth-and-death.

the algorithm given in Table 3. Following this procedure, the proposition kernel is given by :

$$Q(S \to A) = p_b \int_U \frac{1}{\lambda(F)\,\lambda(K)}\,\mathbf{1}_F(S \cup s')\,d\lambda(s') \;+\; p_d \sum_{s' \in S} \frac{1}{n(S)}\,\mathbf{1}_F(S \setminus s') \quad (24)$$

where $U = [F \times K]$, $K = [0, \pi] \times [L_{min}, L_{max}]$ denotes the mark space, λ the Lebesgue measure, and $n(S)$ the number of segments in S.

Then, for $A \subset N_n^f$ ($\equiv$ { sets of n segments }) and $B \subset N_{n+1}^f$:

$$\begin{aligned} \int_A \int_B \pi(dS) Q(S \to dS') &= \int_A f(S) \int_U \mathbf{1}_B(S \cup s') \frac{p_b}{\lambda(F)\,\lambda(K)}\,\lambda(ds')\,\mu(dS) \\ &\text{and} \\ \int_B \int_A \pi(dS) Q(S \to dS') &= \int_B f(S)\,p_d \sum_{s' \in S} \frac{1}{n(S)}\,\mathbf{1}_A(S \setminus s')\,\mu(dS) \end{aligned}$$

Considering the following symmetrical measure ψ on $A \subset N_n^f$ and $B \subset N_{n+1}^f$:

$$\begin{aligned} \psi(A, B) &= \int_A \int_U \mathbf{1}_B(S \cup s')\,\frac{\lambda(ds')}{\lambda(K)}\,\mu(dS) \\ \psi(B, A) &= \int_B \sum_{s' \in S} \mathbf{1}_A(S \setminus s')\,\mu(dS) \end{aligned}$$

where μ denotes the Poisson measure and λ the Lebesgue measure,

and considering uniformly distributed marks in $\lambda(K)$ (that is to say $\frac{\lambda(ds')}{\lambda(K)}$ is the measure of a marked point), the derivative for $(S, S \cup s')$ with respect to ψ is given by :

$$\mathcal{D}^{\pi Q}(S, S \cup s') = f(S)\,\frac{p_b}{\lambda(K)} \quad (25)$$

and the derivative for $(S, S \setminus s')$ with respect to ψ is :

$$\mathcal{D}^{\pi Q}(S, S \setminus s') = f(S)\,\frac{p_d}{n(S)} \quad (26)$$

Finally, the ratio for a death or a birth is computed by equation (22) and is given in Table 3.

4.2.2 Simple Moves

The second move usually proposed is the modification of a randomly chosen object according to a symmetrical transformation.

Let be $\mathcal{T} = \{T_a : a \in E\}$ a family of transformations, parameterized by a vector $a \in E$. The modification of an object s is done by applying T_a :

$$s \leftarrow T_a(s)$$

where a is uniformly chosen in E.

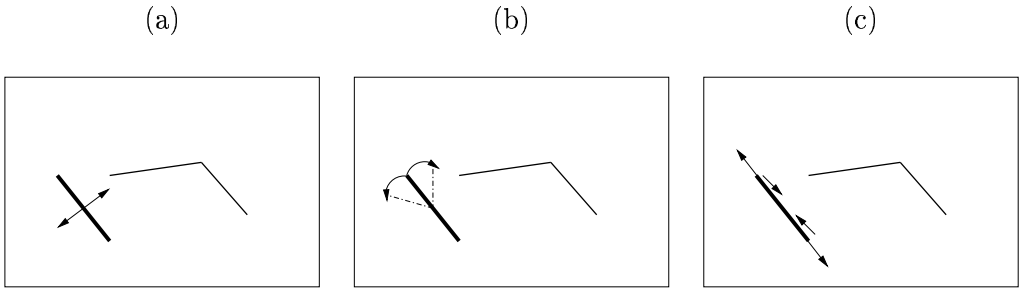

Figure 11: Simple moves : (a) translation - (b) rotation - (c) dilation.

For instance, $\mathcal{T}$ can be defined as the family of rotations defined in $[-\Delta_\theta, \Delta_\theta]$. A rotation T_{d_θ} is defined by :

$$T_{d_\theta}\left(s = \begin{bmatrix} x \\ y \\ L \\ \theta \end{bmatrix}\right) = \begin{bmatrix} x \\ y \\ L \\ (\theta + d_\theta)\,[\pi] \end{bmatrix}$$

where $d_\theta \in [-\Delta_\theta, \Delta_\theta]$ denotes the difference of orientations between the segment s and $T_{d_\theta}(s)$, and $[.]$ denotes the modulo function.

In the same way, families of translations - parameterized by a vector $[dx, dy]$, $dx \in [-\Delta_x, \Delta_x]$, $d_y \in [-\Delta_y, \Delta_y]$ - and dilations - parameterized by $d_L \in [-\Delta_L, \Delta_L]$ - are defined. A translation $T_{[dx,dy]}$ corresponds to the translation of the midpoint

of the considered segment s with the condition that the new midpoint is in $F = [0, X_{max}] \times [0, Y_{max}]$:

$$T_{d_{[dx,dy]}} \left(\begin{bmatrix} x \\ y \\ L \\ \theta \end{bmatrix} \right) = \begin{bmatrix} (x + d_x)\,[X_{max}] \\ (y + d_y)\,[Y_{max}] \\ L \\ \theta \end{bmatrix}$$

A dilation T_{d_L} corresponds to the modification of the segment length by the addition of d_L with the additional condition that the new length is in $[L_{min}, L_{max}]$:

$$T_{d_L} \left(\begin{bmatrix} x \\ y \\ L \\ \theta \end{bmatrix} \right) = \begin{bmatrix} x \\ y \\ L_{min} + (L - L_{min} + d_L)\,[L_{max} - L_{min}] \\ \theta \end{bmatrix}$$

At step t, $S_t = S$.

1. Choose $s \sim \mathcal{U}\{ S\}$

2. Uniformly draw the parameter a of the application T_a

2. Apply T_a on s : $s' = T_a(s)$

3. Compute $R(S, (S \setminus s) \cup s') = \dfrac{f(S, (S \setminus s) \cup s')}{f(S)}$

4. Move to the state $S' = (S, (S \setminus s) \cup s')$ with probability $\alpha = \min(1, R(S.S'))$

Table 4: Transformation of an object by a symmetrical application T_a.

The procedure is the same for each family of symmetrical transformations and is given in Table 4. The proposition kernel for a uniform distribution of a in E is then :

$$Q(S \to A) = \int_E \sum_{s' \in S} \mathbf{1}_A((S \setminus s') \cup T_a(s'))\, \frac{\lambda(da)}{\lambda(E)} \tag{27}$$

The following rule for each transformation :

$$\left\{ \begin{array}{rcl} a \in E & \Longleftrightarrow & -a \in E \ \text{, and} \\ s = T_a(s') & \Longleftrightarrow & s' = T_{-a}(s) \end{array} \right\}$$

allows us to easily define a symmetrical measure ψ on $\Omega \times \Omega$:

$$\begin{aligned} \psi(A,B) &= \int_\Omega \int_E \sum_{s' \in S} \mathbf{1}_A(S)\, \mathbf{1}_B(\underbrace{(S \setminus s') \cup T_a(s')}_{S'})\, \frac{\lambda(da)}{\lambda(E)}\, \mu(dS) \\ &= \int_\Omega \int_E \sum_{s \in S'} \mathbf{1}_A((S' \setminus s) \cup T_{-a}(s'))\, \mathbf{1}_B(S')\, \frac{\lambda(da)}{\lambda(E)}\, \mu(dS') \\ &= \int_\Omega \int_{\{a'=-a/a \in E\}=E} \sum_{s \in S'} \mathbf{1}_A((S' \setminus s) \cup T_{a'}(s'))\, \mathbf{1}_B(S')\, \frac{\lambda(da')}{\lambda(E)}\, \mu(dS') \\ &= \psi(B,A) \end{aligned} \tag{28}$$

Due to equations(27) and (28), the density of $\pi(dS)\, Q(S \to dS')$ with respect to ψ is equal to $f(S)$ and the Green's ratio is the ratio between the two density values :

$$R(S, (S \setminus s) \cup s') = \frac{f((S \setminus s) \cup s')}{f(S)} \tag{29}$$

4.2.3 Birth-and-death within a neighborhood

In order to accelerate the process, it is important to make relevant propositions. Here, the segments are supposed to be connected. So, proposing a birth near a extremity seems to be relevant. That is the reason why we have introduced a birth-and-death kernel within a neighborhood with respect to the connection. It has already been done in [21], but in a complicated way which induces approximations. Our procedure is similar to the one proposed in [23] and is given in Table 5. The transition kernel for a birth-and-death within a neighborhood is composed of two parts, Q_b and Q_d, - as for a uniform birth-and-death (see equation (23)) - respectively correspond to Part 2 and Part 3 of the algorithm. This proposition kernel is more complex than the one of simple birth-and-death and so Green's ratio computation is more complex too. The chosen methodology has been inspired by the one proposed in [13] and is given in details hereafter.

At step t, $S_t = S$.

1. Choose a birth within a neighborhood with a probability p_b. In this case go to 2, otherwise go to 3.

2. Birth case :

- choose a segment $s \sim \mathcal{U}\{ S \}$

- choose an endpoint $e_{s,i} \sim \mathcal{U}\{$ endpoints of s inside the data image $\}$

- sample $z = \begin{bmatrix} d \sim \mathcal{U}[0, \epsilon] \\ \phi \sim \mathcal{U}[0, 2\pi] \\ \theta \sim \mathcal{U}[0, 2\pi] \\ L \sim \mathcal{U}[L_{min}, L_{max}] \end{bmatrix} \xrightarrow{\eta_{s,i}} s' = \begin{bmatrix} e^1_{s,i} + d\cos\phi \\ e^2_{s,i} + d\sin\phi \\ L \\ \theta \end{bmatrix}$

- evaluate Green's ratio R and move to the state $S' = S \cup s'$ with probability $\alpha = \min(1, R)$

3. Death case :

- choose $s \sim \mathcal{U}\{ \mathcal{V}_c \}$, where $\mathcal{V}_c$ is the subset of connected segments in S

- evaluate Green's ratio R and move to the state $S' = S \setminus s$ with probability $\alpha = \min(1, R)$

Table 5: Birth and Death within a neighborhood.

Birth part of the proposition kernel :

$$Q_b(S \to A) = \sum_{s \in S} p^S(s) \sum_{i=1}^{2} p^s(e_i)\, q_b^{s,e_i}(S \to A) \tag{30}$$

where $p^S(s)$ is the probability of choosing s in S, $p^s(e_i)$ is the probability of choosing the endpoint e_i of s and $q_b^{s,e_i}(S \to A)$ the probability of moving from S to A with a birth from e_i.

The simplest choice for p^S and $p^s(e_i)$ is the uniform distribution, so that :

$$p^S(s) = \frac{1}{n(S)}$$

where $n(S)$ is the number of segments in S.

Given that a segment is not supposed to be connected outside of the compact set F corresponding to the data, we take the following distribution for the choice of the endpoint given a segment s :

$$p^s(e_i) = \begin{cases} \frac{1}{2} & \text{if the two endpoints of } s \text{ are falling in } F. \\ 0 & \text{if the endpoint } e_i \text{ of } s \text{ is not in } F. \\ 1 & \text{if } e_i \text{ is the only endpoint of } s \text{ falling in } F. \end{cases}$$

Then, we have to define $q_b^{s,e_i}(S \to A)$. The procedure to propose a birth of segment from e_i is the one defined in Table 5. Firstly, the endpoint of the proposed segment is randomly drawn in the ball of center e_i and of radius ϵ. Secondly, the orientation and the length are uniformly drawn in the mark space[4]. From the randomly drawn vector z thus defined, we finally apply a diffeomorphism $\eta_{s,i}$ in order to compute the corresponding segment $s' = \eta_{s,i}(z)$. Consequently, the probability $q_b^{s,e_i}(S \to A)$ can be written as follows :

$$q_b^{s,e_i}(S \to A) = P_Z((S \cup \eta_{s,i}(Z)) \in A)$$

where $Z \sim \mathcal{U}[\underbrace{[0,\epsilon] \times [0,2\pi] \times [0,2\pi] \times [L_{min}, L_{max}]}_{\Sigma}]$

[4]In the case of the two last models, the orientation is drawn so that the angle formed by the two connected segments is large because of the new definition of the connection.

Then,

$$\begin{aligned} q_b^{s,e_i}(S \to A) &= \int_\Sigma \mathbf{1}_A(S \cup \eta_{s,i}(z)) \, \frac{\lambda(dz)}{\lambda(\Sigma)} \\ &= \int_{\eta_{s,i}(\Sigma)} \mathbf{1}_A(S \cup s') \, \underbrace{|J_{\eta_{s,i}^{-1}(s')}|}_{\frac{1}{d_e(s,s')}} \, \frac{\lambda(ds')}{\lambda(\Sigma)} \\ &= \frac{1}{\lambda(\Sigma)} \int_U \mathbf{1}_{V(s,e_i)}(s') \, \mathbf{1}_A(S \cup s') \, \frac{1}{d_e(s,s')} \, \lambda(ds') \end{aligned}$$

where λ denotes the Lebesgue measure, J the Jacobian, $d_e(s,s')$ the distance between the two connected endpoints of s and s', and $V(s,e_i)$ the set of segments with at least one endpoint closer than ϵ to the endpoint e_i of s.

Finally, the expression of the birth part is the following :

$$Q_b(S \to A) = \frac{1}{n \, \lambda(\Sigma)} \sum_{s \in S} \sum_{i=1}^{2} p^s(e_i) \int_U \mathbf{1}_{V(s,e_i)}(s') \, \mathbf{1}_A(S \cup s') \, \frac{1}{d_e(s,s')} \, \lambda(ds') \quad (31)$$

Death part of the proposition kernel :

$$Q_d(S \to A) = \sum_{s' \in S} p_d^S(s') \, \mathbf{1}_A(S \setminus s') \quad (32)$$

where $p_d^S(s)$ is the probability of choosing s in S for a death. We define this probability by taking a uniform distribution on the segments which could be drawn by a birth within a neighborhood, that is to say segments which are connected :

$$p_d^S(s') = \begin{cases} \dfrac{1}{\mathrm{card}(\mathcal{V}_c(S))} = \dfrac{1}{n(S) - n_f(S)} & \text{if } s' \in \mathcal{V}_c(S) \\ \\ 0 \text{ if s' is free.} \end{cases}$$

where $\mathcal{V}_c(S)$ is the set of connected segments in S.

Radon-Nykodym derivative :

In order to verify the detailed balance condition, a symmetrical measure ψ on $A \subset N_n^f \times \subset N_{n+1}^f$ is defined :

$$\begin{aligned}\psi(A,B) &= \int_A \int_U \mathbf{1}_B(S \cup s')\, \mathbf{1}_{\mathcal{V}_c^{S\cup s'}}(s')\, \nu(ds')\, \mu(dS) \\ \psi(B,A) &= \int_B \sum_{s' \in S} \mathbf{1}_{\mathcal{V}_c^S}(s')\, \mathbf{1}_A(S \setminus s')\, \mu(dS)\end{aligned}$$

where $U = F \times [0,\pi] \times [L_{min}, L_{max}]$, $\mathcal{V}_c^S$ denotes the set of connected segments in S, μ the Poisson measure and ν the measure of a marked point. Considering uniformly distributed marks in K, this measure is : $\nu(ds) = \dfrac{\lambda(ds)}{\lambda(K)}$, where λ is the Lebesgue measure.

Note that, by the Radon-Nykodym theorem, $\pi(.)\, Q(. \to .)$ is absolutely continuous with respect to ψ. Indeed, $\psi(A,B) = 0 \Rightarrow \ \pi(A)\, Q(A \to B) = 0$, for $A \subset N_n^f$ (resp.N_{n+1}^f) and $A \subset N_{n+1}^f$ (resp. N_n^f).

The equation (31) allows to write for $A \subset N_n^f$ and $B \subset N_{n+1}^f$:

$$\begin{aligned}\int_A \int_B \pi(dS)\, Q(S \to dS') &= \int_A f(S) \int_U \mathbf{1}_B(S \cup s') \frac{p_b}{n(S)\, \lambda(\Sigma)} \sum_{u \in S} \sum_{i=1}^{2} \mathbf{1}_{V(s',e_i)}(u)\, \frac{p^u(e_i)}{d_e(u,s')}\, \lambda(ds')\, \mu(dS) \\ &= \frac{p_b\, \lambda(K)}{n(S)\, \lambda(\Sigma)} \int_A \int_U \mathbf{1}_B(S \cup s')\, \mathbf{1}_{\mathcal{V}_c^{S\cup s'}}(s') \left[f(S) \sum_{i=1}^{2} \sum_{u \in V(s',e_i)} \frac{p^u(e_i)}{d_e(u,s')} \right] \nu(ds')\, \mu(dS)\end{aligned}$$

Thus, the derivative for $(S, S \cup s')$ with respect to ψ is :

$$\mathcal{D}^{\pi Q}(S, S \cup s') = f(S)\, \frac{p_b\, \lambda(K)}{n(S)\, \lambda(\Sigma)} \sum_{i=1}^{2} \sum_{u \in V(s',e_i)} \frac{p^u(e_i)}{d_e(u,s')} \tag{33}$$

Furthermore, using equation (32) we have :

$$\int_B \int_A \pi(dS) Q(S \to dS') = \int_B f(S)\, p_d \sum_{s' \in S} p_d^S(s')\, \mathbf{1}_A(S \setminus s')\, \mu(dS)$$

As $p_d^{S'}(s) = 0$ if s is free, and $p_d^{S'}(s) = \frac{1}{n(S')-n_f(S')}$ otherwise, this can be written as follows :

$$\int_B \int_A \pi(dS) Q(S \to dS') = \int_B \sum_{s' \in S} \mathbf{1}_{\mathcal{V}_c^S}(s')\, \mathbf{1}_A(S \setminus s') \left[f(S)\, p_d\, \frac{1}{n(S) - n_f(S)} \right] \mu(dS)$$

Thus, the derivative for $(S, S \setminus s')$ with respect to ψ is :

$$\mathcal{D}^{\pi Q}(S, S \setminus s') = f(S)\, \frac{p_d}{n(S) - n_f(S)} \tag{34}$$

Finally, using equations (22), (33) and (34), the Green's ratio for the birth of a segment s is the following :

$$\boxed{R_b(S, S') = \frac{f(S')}{f(S)}\, \frac{p_d}{p_b}\, \frac{\lambda(\Sigma)}{\lambda(K)}\, \frac{n(S)}{n(S') - n_f(S')}\, \frac{1}{\sum_{i=1}^{2} \sum_{u \in V(s,e_i)} \frac{p^s(e_i)}{d_e(u,s)}}} \tag{35}$$

where $S' = (S \cup s)$.

Likewise, the Green's ratio for the death of a segment s is :

$$\boxed{R_d(S, S') = \frac{f(S')}{f(S)}\, \frac{p_b}{p_d}\, \frac{\lambda(K)}{\lambda(\Sigma)}\, \frac{n(S) - n_f(S)}{n(S')}\, \Big(\sum_{i=1}^{2} \sum_{u \in V(s,e_i)} \frac{p^s(e_i)}{d_e(u,s)}\Big)} \tag{36}$$

where $S' = (S \setminus s)$.

4.3 Diagnosing convergence in practice

A stopping rule to guarantee convergence of the chain $\{S_t\}$ to the stationary measure has to be defined. To detect this convergence, the convergence of the empirical average(s) M^k of some function(s) k on S_t is usually evaluated in the implementation of MCMC algorithms (see [17]). A corresponding algorithm is proposed in Table 6. For a given number n_{test} of iterations, we test (for each function k) if the absolute difference between the empirical average M_t^k, evaluated at iteration t, and M_{ref}^k, the last average which has not verified the test, is lower than a small constant δ (after a minimal iteration number, t_{min}). If the test is verified for n_{test} iterations, then the algorithm is stopped.

1. $n = 1$

2. RJMCMC step t

3. If $t \geq t_{min}$,

a. Evaluate empirical average of each function k : $M_t^k = \dfrac{(n-1)\, M_{t-1}^k + k(S_t)}{n}$

b. $\begin{cases} \text{If } |M_t^k - M_{ref}^k| < \delta \quad \forall k\,, \quad T = T + 1 \\ \text{Else, } T = 0 \text{ and } M_{ref}^k = M_t^k \end{cases}$

4. If $T = n_{test}$, stop

Else $\begin{cases} n = n + 1 \\ t = t + 1 \end{cases}$ and go to 2.

Table 6: Stopping rule for the RJMCMC algorithm.

In our case, the degree of correlation between the S_t is very strong : propositions of transition may often be refused and moves concern only small modifications of the configuration. However, we can use sub-sampling to reduce the effect of the autocorrelation of $\{S_t\}$. So, the chosen stopping rule is based on the empirical mean of a sub-sampling of $\{S_t, t = 1...N\}$ given by :

$$Y = \{\, S_t \in \{S_t, t = 1...N\} \,/\, t = 1\ [T]\,\}$$

where T is a fixed period between two samples of Y with respect to $\{S_t\}$.

4.4 Samples of the prior models

In this subsection, a comparison of prior models is done from samples of each distribution obtained by the RJMCMC algorithm described in subsection 2, using the stopping rule given in Table 6. Precisely, the chosen proposition kernel is composed by two equiprobable kernels : a uniform birth-and-death kernel with $p_b = 1/2$ and a birth-and-death within a neighborhood kernel with $p_b = 1/2$. Some tests have been realized by taking only uniform birth-and-death kernel but, in this case, the stationarity is reached after much more iterations or is never reached. This fact is also

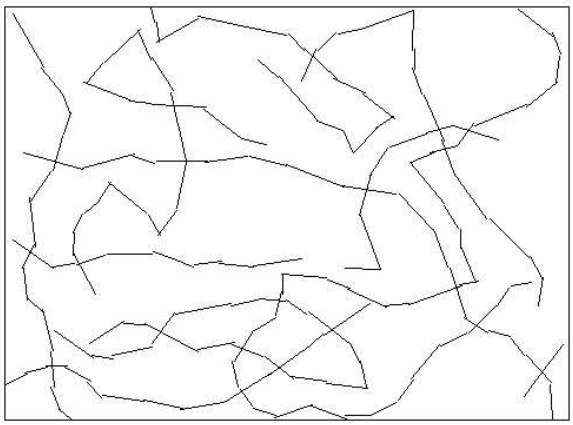

Figure 12: Sample of the "Candy" model whose density, with respect to Poisson process of intensity 40000, is defined by the following parameterization : $\beta = 1$, $w_f = 35$, $w_s = 15$, $w_{io} = 50$, $w_{eo} = 50$.

pointed out in [23] and one can understand this due to the strong geometrical constrains imposed on the process. The initial state is the empty configuration, except for the "IDQ" model where it is taken from the independent uniform distribution. The stationarity has been evaluated through the convergence of different statistics for each model. For the "Candy" model, the convergence of empirical averages of the sufficient statistics $n(S)$, $n_s(S)$, $n_f(S)$, $n_{io}(S)$ and $n_{eo}(S)$, is tested following table 6. For the "Quality Candy" model and the "IDQ" model, the sum of clique qualities are also tested (for the "IDQ" model , the number of pairs of connected segments $n_c(S)$ replaces $n_s(S)$ and $n_f(S)$). To compute empirical averages a sub-sampling is realized by selecting one sample every 1000 RJMCMC steps (after a minimal number of iterations fixed at 10000 iterations).

First of all, a result of the "Candy" model is given in Figure 12. The density specifying this process, with respect to Poisson process of intensity 40000, is defined by the following weights : $\beta = 1$, $w_f = 35$, $w_s = 15$, $w_{io} = 50$ and $w_{eo} = 50$. The result seems good in the sense that all segments are connected and form long broken lines. Nevertheless, the drawback of this model, mentioned in Section 2.1, is confirmed : small breaks between extremities are visible and the curvature of lines

can be extremely strong. The result of this is a line network not as smooth as can be a road in reality. This sample corresponds to the last sample of the RJMCMC algorithm whose empirical averages are plotted in Figure 15(a). The stationarity is reached after 1663000 iterations which corresponds to a computing time of 1 minute and 46 seconds (on a PC with a Pentium III processor, 1000 MHz, and 1024 Mo of RAM) .

Figure 13 gives realizations of processes specified by a density of type "Quality Candy". The first one, 13(a), is the uniform Poisson process. The empirical average of the number of points $n(s)$ is verified to be equal to $\beta\,\lambda$ (if the measure of the compact set F is taken equal to 1), where λ is the intensity of the reference Poisson process. This allows to check the correct progress of the used RJMCMC algorithm. Plot 13(b) concerns a realization without the internal bad orientation, but with the connection trough the number of free and single segments. In this case, as the connection is only defined for a large angle, the process is not stable. In practice, it results in more and more segments sticking together. It is the case for Plot 13(b), which is the last sample of the algorithm not stopped by averages convergence but by the iteration number, whereas all other examples have been obtained after the stationarity detection. Then, Plot 13(c) gives an example without the quality of connection. It looks like a sample of "Candy" model without the connections at sharp angle. The complete model is given by Plot 13(d). The line network is smoother than the one of the "Candy" model. It seems to be better applied to road detection. Figure 15 (b) gives the associated statistics. This process has converged after less iterations (1354000) than the "Candy" process but in more time (2 minutes). Indeed, the cost of density computation is higher in this case than for the "Candy" density.

Finally, Figure 14 deals with the "IDQ" model. Plot 14(a) shows a drawback of this model : if the weight assigned to the quality of connection is reduced to zero, a segment tends to be connected to two other segments by one of its extremity. Indeed, in this case, the global term of connection intensity increases more by the addition of one segment connected to two others than by the addition of one segment connected to an extremity which was not connected before. Nevertheless, the sample of the complete "IDQ" model, given in Plot 14(b), completely satisfied the goal of simulating roads, providing a very smooth line network. Moreover, Plot (c) of Figure 15 shows that the RJMCMC algorithm (Plot 14(b) corresponds to its last sample) has converged in less time and less iterations than the two other ones : 15552000 iterations and 1 minute and 36 seconds. So, the density computation seems to be

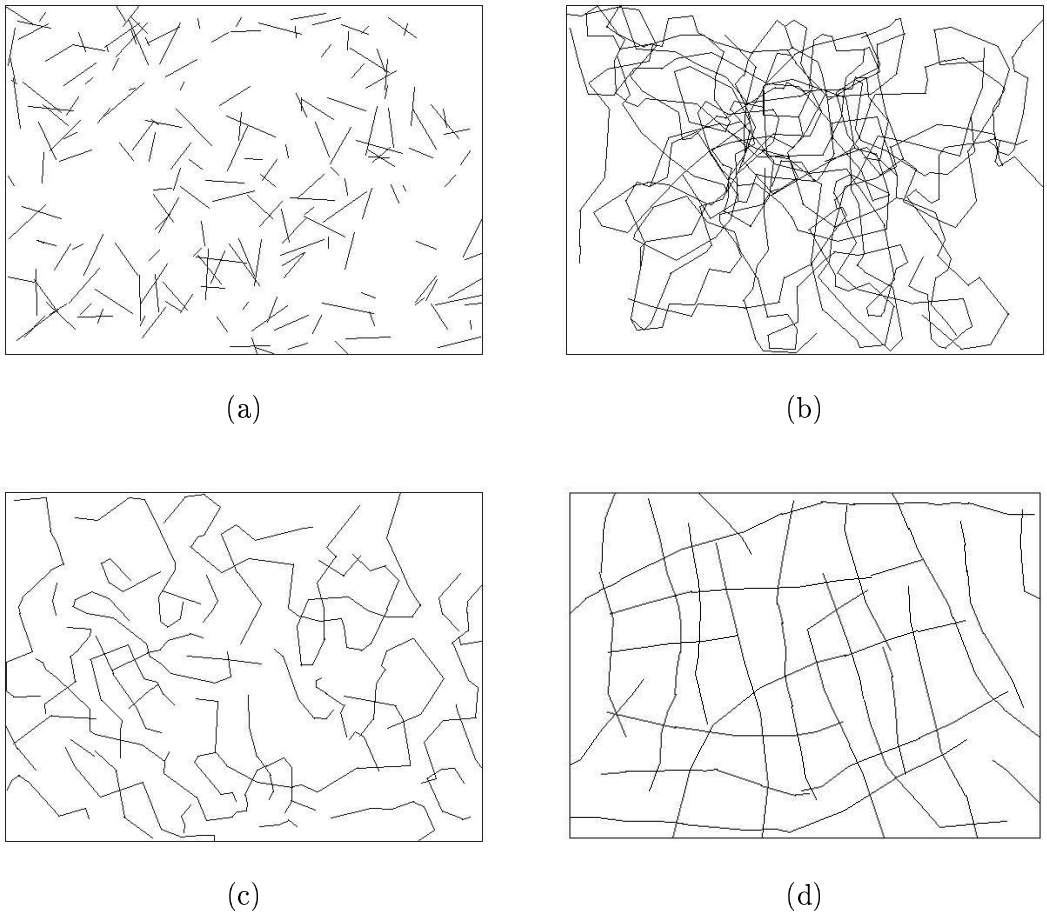

Figure 13: Samples of the "Quality Candy" Model - (a) Process without interaction : $\omega_i = 0 \, \forall i$ - (b) Process only depending on segment states : $\omega_f \neq 0$, $\omega_f \neq 0$, $\omega_r = \omega_c = 0$ - (c) Process depending on segment states and on external bad orientation : $\omega_c = 0$ - (d) Complete model.

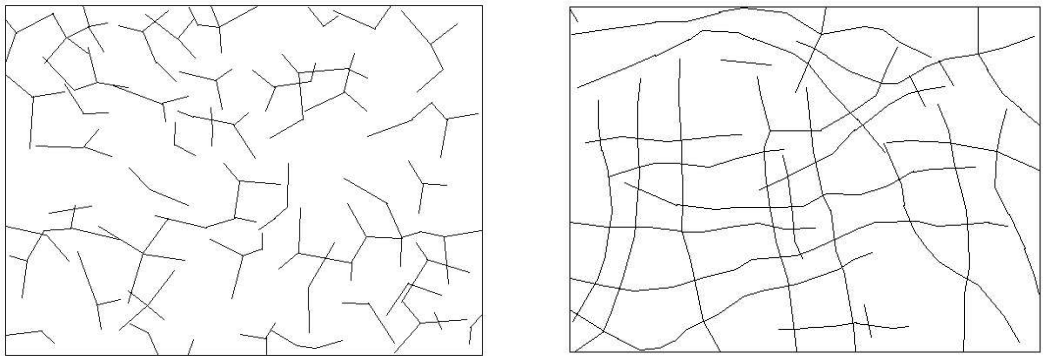

(a) (b)

Figure 14: Samples of the "IDQ" model - (a) Model with $\gamma_Q = 0$, where γ_Q is the weight of the connection quality in the energy - (b) Complete model.

equivalent to the one of the "Candy" model. Yet, the number of iterations is not so good because the initial configuration is taken from a uniform and independent law instead of the empty configuration as for the two other cases. Indeed, the initial state cannot be the empty configuration because, if potential weights are too important, the Markov chain will stay in the empty state. Here, to obtain a relevant configuration, weights have to be stronger than for the two first models because quantities evaluated - intensity, density, quality - are averages on the whole configuration[5].

4.5 Simulated Annealing

In order to achieve the goal of extracting road networks from images, we have to estimate a configuration which maximize the density of the process with respect to the Poisson process measure, given by equation (1). If we had defined a proper likelihood, we would have talked about MAP estimation [6]. A possible alternative is given in [18]. It is more sensible to details than the MAP criterion, but making use

[5]When the object number is important, the modification of averages I, D and Q is low. But this is not the case when the number of objects is low, which explains the fact that the number of objects cannot arise from the empty state.

[6]We are not in a Bayesian framework because of the construction of the data term which does not correspond to a family of known probability densities.

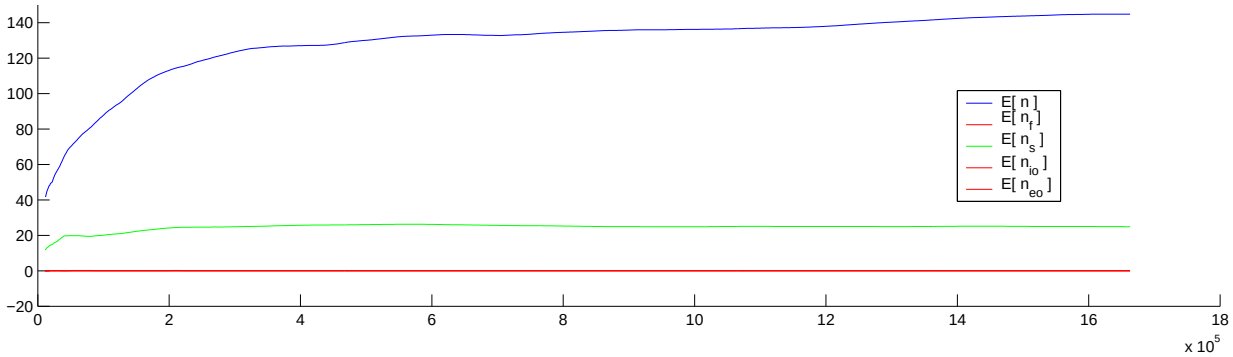

(a) Averages convergence detected after 1663000 iterations/106 s. for the "Candy" model.

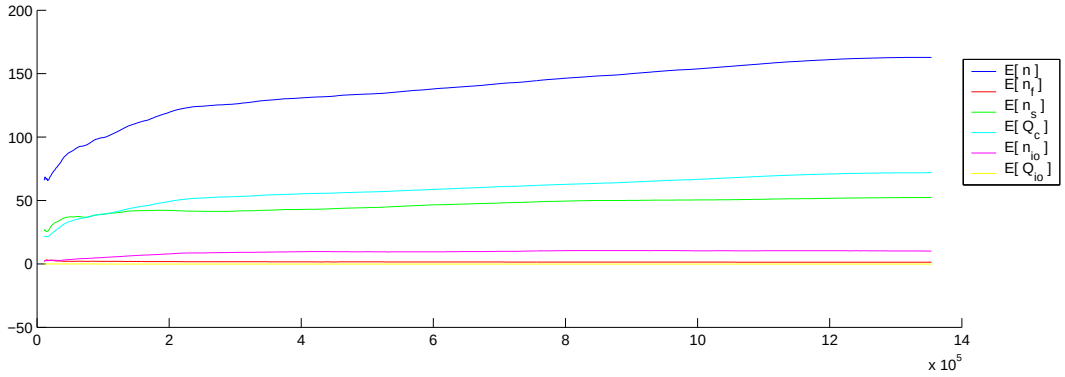

(b) Averages convergence detected after 1354000 iterations/120 s. for the "Quality Candy" model.

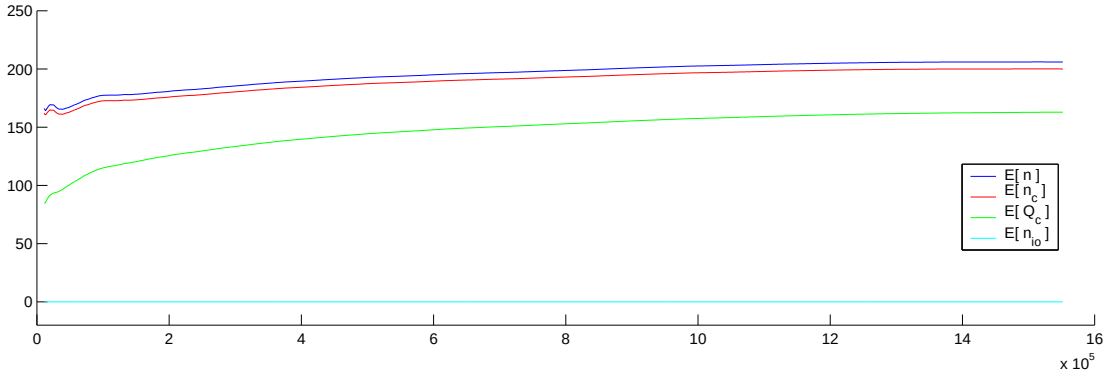

(c) Averages convergence detected after 1552000 iterations/96 s. for the "IDQ" model.

Figure 15: Plots of statistics evaluated from generated samples by RJMCMC algorithm - (a) "Candy" Model - (b) "Quality Candy" model - (c) "IDQ" model.

of it is more difficult and it requires more calculation.

The optimization is realized by a simulated annealing using the RJMCMC algorithm given in Table 2 with a proposition kernel composed of five equiprobable kernels : uniform birth-and-death ($p_b = 1/2$), birth-and-death within a neighborhood ($p_b = 1/2$), rotation, translation and dilation. The algorithm is given in Table 7.

Successive simulations of $f_T(S)\mu(dS)$ obtained by a RJMCMC algorithm (see Table 2) where : $$f_T(S) \propto [h_d(S)h_p(S)]^{1/T}$$ with T gradually dropping to 0.

Table 7: simulated annealing with a RJMCMC algorithm.

A proof of convergence is given in [22] for a simulating annealing with a Birth and Death sampler when the decrease of temperature T is logarithmic. This proof can be adapted to RJMCMC algorithm. In practice, temperature decreases geometrically in order to accelerate the algorithm, and at each step :

$$T_{n+1} = c\, T_n$$

where c denotes a constant close to 1.

5 Results

In this section, results of road detection for each prior models are compared on several types of data. For a given image, the data term, given by equation (13), is taken identical for all the models. The optimization, realized by a simulated annealing with a RJMCMC algorithm, is the one described in Section 4.5.

5.1 Results on a SPOT image

The first image - see Figure 16 - is a SPOT image without any major difficulty : the line network is rectilinear and clearly contrasted with respect to the background.

Thresholds t_1 and t_2 of data potential (eq. (16)) are empirically chosen equal to $t_1 = 4$ and $t_2 = 8$.

Figure 16: Data 1 : a SPOT image (256×256 pixels).

Figure 17 gives results for the "Candy" model with two different decreasing laws of the temperature. If it is too fast, the detected line network is not complete as Figure 17(b) shows. Indeed, there is a critical temperature where it is important to pass slowly in order to reach the global maximum of the density (Figure 17(b) is only a local minimum). That is why the complete cross which can be see in Figure 16 is present in Figure 17(a), obtained with a slower temperature decrease. This points out that the algorithm is very dependent on the temperature decrease. Thus, before analyzing results of a prior models, we have to wonder whether we can be confident in our algorithm.

Likewise, Figure 18 gives some results for the " Quality Candy" model. Just as sample of the prior distribution, this model provides a smoother line network. Moreover, it appears to be not as sensitive to the temperature decrease as the "Candy" model. This implies a possible significant reduction of computing time.

Figure 19 supplies results for "IDQ" model. The bad line network given in Figure 19(b) is not improved by a reduction of the temperature decrease, which corresponds to Fig 19(a). Indeed, in the two cases a lot of false alarms and connection at right

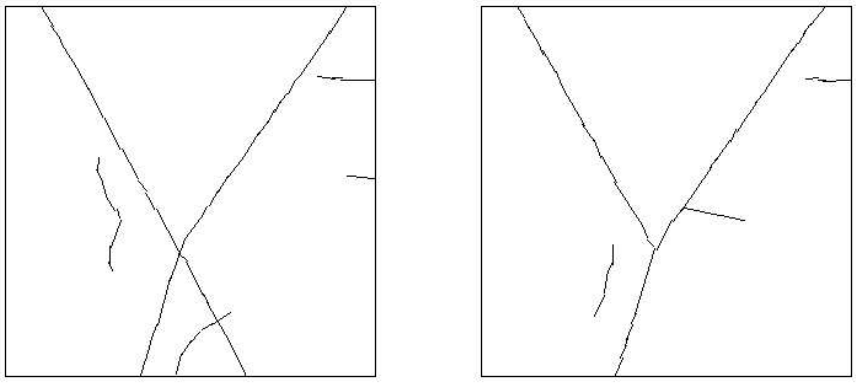

(a) Slow temperature decrease (b) Fast temperature decrease

Figure 17: Results of line network extraction from SPOT image (Fig. 16) taking the "Candy" model to define the prior density of the point process - (a) geometric decrease of T with $c = 0.999999$ - (b) geometric decrease of T with $c = 0.99999$.

angle are present. This can be explained by the definition of connection intensity which is a mean on all the configuration. Indeed, free segments are allowed as soon as they are counter-balanced by segments which are connected with more than two segments.

5.2 Results on an aerial image

In this section, the line network extraction is realized on an aerial image. The task is not straightforward here, owing to geometrical noise, that is to say noise characteristic to the observed scene. Indeed, some trees interfere with good detection of road sections ; some fields have nearly the same grey level value as the roads ; and field textures could well reply to the statistical test used to compute the data term if the segment width is chosen too small. Each prior model is tested with a more or less strong weight with respect to the data term. The latter is the same for each model, with $t_1 = 8$ and $t_2 = 15$. From now on, the temperature of the algorithm is decreased geometrically with $c = 0.999999$.

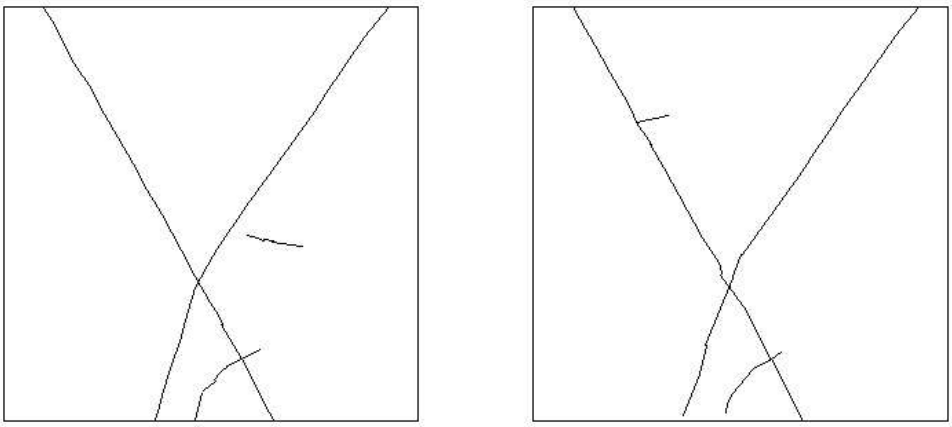

(a) Slow temperature decrease (b) Fast temperature decrease

Figure 18: Results of line network extraction from SPOT image (Fig. 16) taking the "Quality Candy" model to define the prior density of the point process - (a) geometric decrease of T with $c = 0.999999$ - (b) geometric decrease of T with $c = 0.99999$.

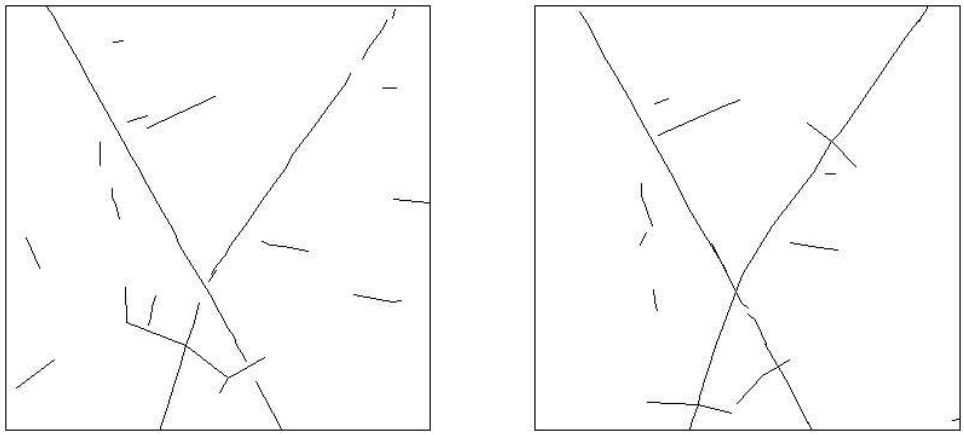

(a) Slow temperature decrease (b) Fast temperature decrease

Figure 19: Results of line network extraction from SPOT image (Fig. 16) taking the "IDQ" model to define the prior density of the point process - (a) geometric decrease of T with $c = 0.999999$ - (b) geometric decrease of T with $c = 0.99999$.

Figure 20: Data 2 : aerial image (892×652 pixels).

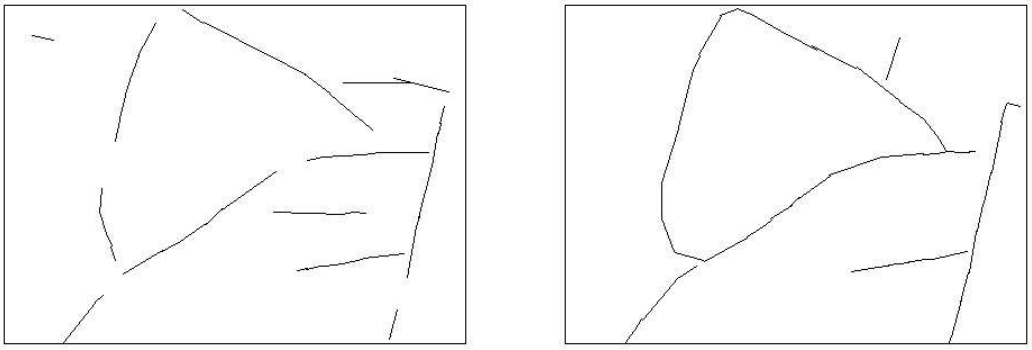

(a) With strong data term (b) With strong prior term

Figure 21: Results of line network extraction from Fig. 20 taking the "Candy" model to define the prior density of the point process - (a) with a strong data term - (b) with a strong prior term.

Figure 21 gives two estimates obtained by simulating annealing with a RJMCMC algorithm (see section 4.5) for a low prior term in Figure 21(a) and a strong one in Figure 21(b). The first one provides a result with just one false alarm but is incomplete. The line network 21(b) correctly fulfill the prior constraints in the sense that there is no more breaks and false alarms. Nevertheless, this line network is not complete either.

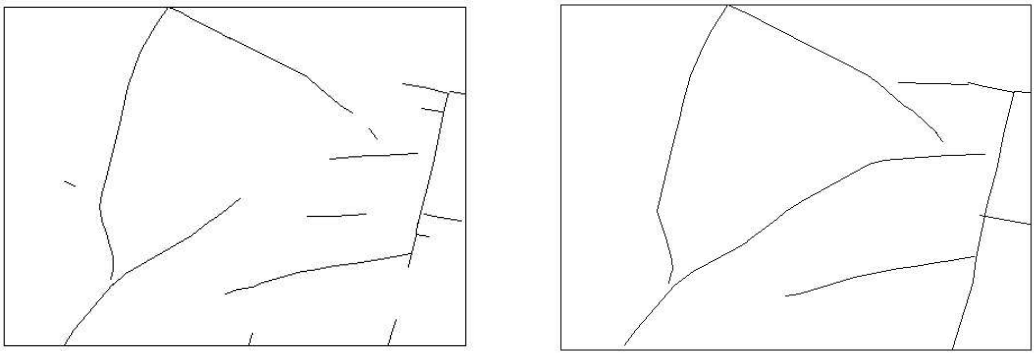

(a) With strong data term (b) With strong prior term

Figure 22: Results of line network extraction from Fig. 20 taking the "Quality Candy" model to define the prior density of the point process - (a) with a strong data term - (b) with a strong prior term.

Figure 22 shows results corresponding to the "Quality Candy" model. Globally, line networks are smoother than in Figure 21. Like in the Figure 21(a), a too strong data term provides an incomplete line network. Then, Figure 22(b) shows that "'Quality Candy" model is well-adapted to this extraction problem. Nearly all the roads are present and there is no more breaks, except if two roads are crossing with a too sharp angle because of strong penalty of internal bad orientation R_{io}. Finally, taking a good compromise between prior term and data term, we obtain a very satisfactory line network given in Figure 23. This could be obtained neither for the "IDQ" model, nor for the "Candy" model. Figure 24 provides results concerning the "IDQ" model. If the prior term gains in weight, a segment connected to many others will appears instead of several double segments, as it is visible in Figure 24(b). It confirms that this model is not well adapted unless we redefine the c_r-cliques of

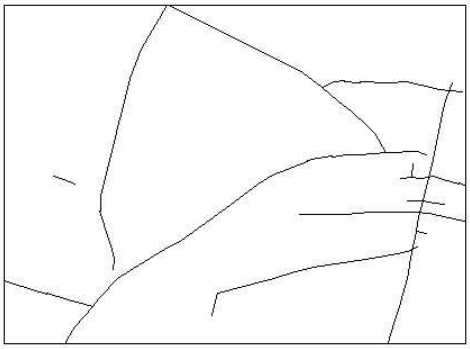

Figure 23: Results of line network extraction from Fig. 20 taking the "Quality Candy" model with a good compromise between data term and prior term.

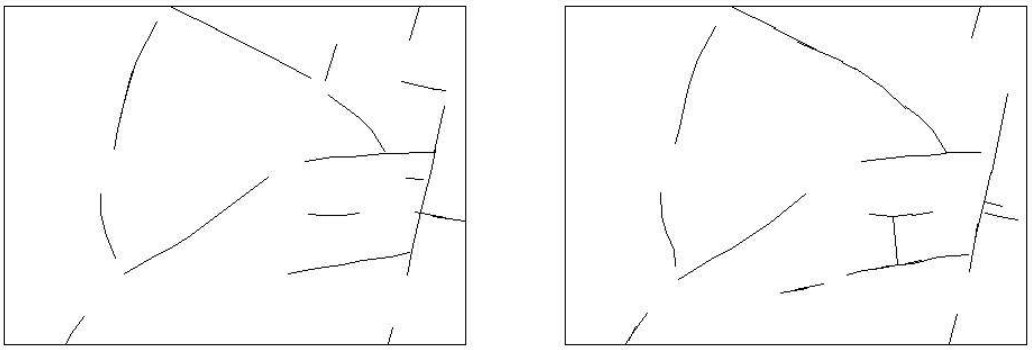

(a) With strong data term (b) With strong prior term

Figure 24: Results of line network extraction from Fig. 20 taking the "IDQ" model to define the prior density of the point process - (a) with a strong data term - (b) with a strong prior term.

connection (for instance, using different clique cardinalities). Moreover, we have a little modified the definition of the quality of a clique because the first results provided only sections of maximal quality (very smooth sections). More precisely, if the value of the function of quality σ is larger than 0.9, the maximal value 1 is assigned to the quality of the clique.

5.3 Results on a radar image

The last image presented in this report is an ERS image of Mexico city whose road network detection is made difficult by radar noise (speckle). Results obtained for each prior models with a strong data term are shown in Figure 25. Detected line networks are satisfactory and show that the data term is well defined as it allows to detect roads in very noisy images (here, $t_1 = 3$, $t_2 = 9$). It is interesting to note that, contrary to the two first road networks in Figure 16 and Figure 20, this one appears to be a possible application for "IDQ" model. Indeed, it presents a lot of crossroads at right angle, which allows many connections for one segment with an endpoint near a crossroad center.

For the "Candy" model, taking a strong prior term does not improve the result of extraction. For the "Quality Candy" model, it allows to avoid entirely breaks in the network as shown in Figure 26. Nevertheless, the result is a little less exhaustive than in 25(c). For the "IDQ" model, we obtain a very smooth line network with many connections at the level of cross roads, and also with breaks and free segments to reach optimal value of intensity.

5.4 Computing Efficiency

This section is devoted to the computing efficiency of each model. For each estimate given in the previous subsections, we give in Table 8 the corresponding number of iterations and the corresponding computing time (on a PC with a Pentium III processor, 1000 MHz, and 1024 Mo of RAM).

One can notice that the computing time arises with the size of the data image, which comes from an increase of object number, especially when the temperature is low. The most time consuming model is the "IDQ" model. The "Quality Candy" converges faster than the "Candy" model on these examples, and thus, whereas the computing time by step is larger, the total computing time is lower.

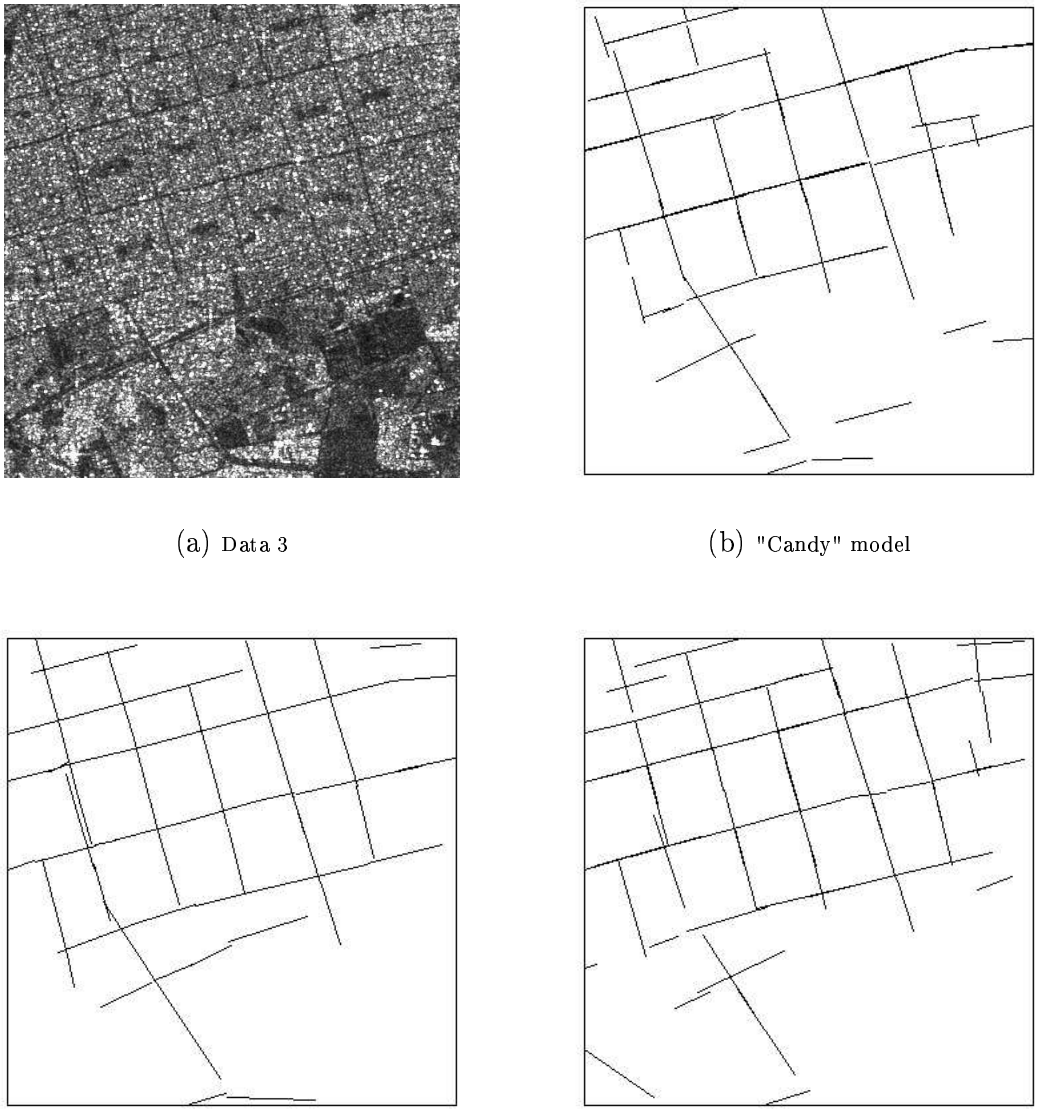

(a) Data 3 (b) "Candy" model

(c) "Quality Candy" model (d) "IDQ" model

Figure 25: Results of line network extraction from a radar image with a strong data term - (a) Data 3 : ERS radar image (525 × 546 pixels) - (b) "Candy" model - (c) "Quality Candy" model - (d) "IDQ" model.

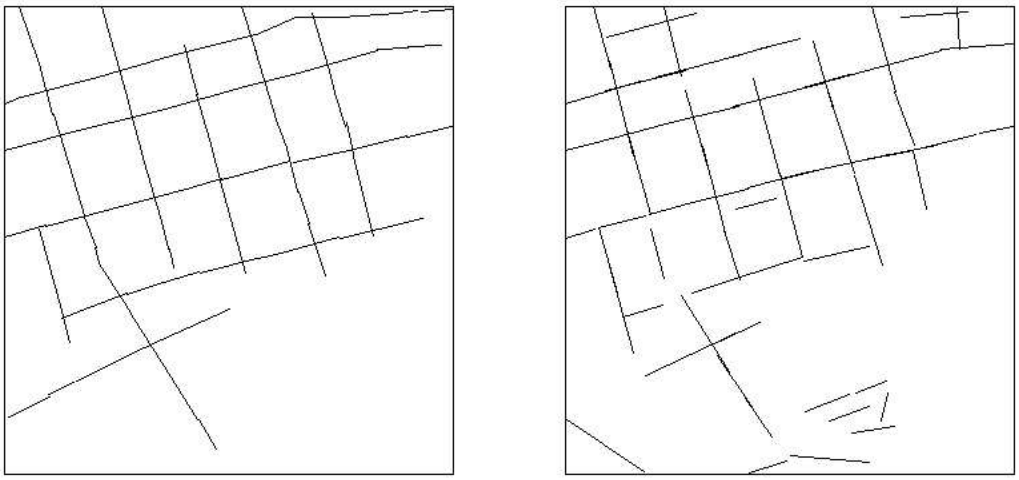

(a) "Quality Candy" model (b) "IDQ" model

Figure 26: Results of line network extraction from Fig. 25(a) with a strong prior term - (a) "Quality Candy" model - (b) "IDQ" model.

	"Candy"	"Quality Candy"	"IDQ"
Data 1 with fast decrease of T	1935000 iterations 5 min 31 s	1600000 iterations 3 min 56 s	6155000 iterations 15 min 21 s
Data 1 with slow decrease of T	3605000 iterations 12 min 28 s	4500000 iterations 11 min 17 s	7165000 iterations 17 min 30 s
Data 2 with strong data term	6820000 iterations 33 min 20 s	4300000 iterations 23 min 10 s	10155000 iterations 40 min 56 s
Data 2 with strong prior	5380000 iterations 26 min 35 s	4395000 iterations 22 min 56 s	10145000 iterations 42 min 33 s
Data 3 with strong data term	8045000 iterations 46min 32 s	5155000 iterations 45 min 37 s	13275000 iterations 1 H 20 min 4 s
Data 3 with strong prior	6065000 iterations 38 min 42 s	5265000 iterations 1 H 10 min 7 s	6065000 iterations 47 min 2 s

Table 8: Computing Time of simulated annealing for each model.

5.5 Summary

Finally, performances of each model in detecting line networks from images are summarized in Table 9. Except for the computing time, it is subjective results, given that we do not have any ground truth to compare with the detected line network. This leads to select the "Quality Candy" model as the most fitted to the application.

	"Candy"	"Quality Candy"	"IDQ"
Time computing	+	+	−−
Smoothness	−	++	++
Exhaustive result	+	++	−
Avoiding false alarms	+	++	−−

Table 9: Summary of the performances of each model. (−) denotes bad performances and (+) good performances.

6 Conclusion and future work

In this report, three point processes - named "Candy", "Quality Candy" and "IDQ" -, specified by a density with respect to the uniform Poisson process, have been presented in order to propose a relevant prior model for line network extraction from images. We have proven local stability of "Quality Candy" model, which has been already done for "Candy" and "IDQ" model [23, 13]. In order to simulate process distribution, we have proposed a reversible jump Markov chain Monte Carlo algorithm, which is based on a composed proposition kernel, which accelerates convergence of the algorithm. The samples generated by the algorithm confirm our choice of prior models. The extraction of line networks has been realized by a simulated annealing

with a RJMCMC algorithm leading to the optimum of the process density composed by a prior density and a data term based on a statistical test. The importance of the speed of the temperature decrease has been pointed out : we had to be near the theoretical decrease to obtain a complete result, which can thus be compared to other ones. The results show that the "IDQ" is not suitable except for road networks which contain crossroads at right angle. Indeed, the fact of working on averages on all the cliques is not realistic. Moreover, the computing time is clearly more important for the "IDQ" model than for the two other prior models. Globally, the "Candy" and "Quality Candy" provide good results avoiding false alarms and are quite exhaustive. The "Quality Candy" model gives smoother results in less computing time on average than the "Candy" model, which justifies the use of a dual potential for the connection. Thus, "Quality Candy" model is the most suited model for the road extraction prior.

As this study has shown that the optimization algorithm has an influence not only on the computing time but also on the final result, we will focus in a near future on the construction of a RJMCMC algorithm with more relevant proposals and on the improvement of the simulated annealing by using an adaptive rule of decrease or using a parallel simulated annealing [1]. Moreover, it would be interesting to extend this study to other types of line networks as rivers or sub-surface networks and other types of models as broken lines or hierarchical models. Finally, criteria of performance have to be defined in order to give a reliable evaluation of detected line networks with respect to a line network provided by an expert [20], after a previous registration [7, 15].

Acknowledgment

The authors would like to thank the French Mapping Institute (IGN) for providing aerial data, the French Space Agency (CNES) for providing SPOT images, the European Space Agency (ESA) for providing ERS images as well as Marie-Colette van Lieshout and Radu Stoica from CWI for several interesting discussions. The first author would like to thank the French Geological Survey (BRGM) for partial financial support.

References

[1] R. Azencott, editor. *Simulated Annealing : Parallelization Techniques*, chapter 4. John Wiley and Sons, 1992.

[2] M. Barzohar and D. B. Cooper. Automatic finding of main roads in aerial images by using geometric-stochastic models and estimation. *IEEE Trans. on PAMI*, 18 - 2:707–721, 1996.

[3] M. A. Fischler, J. M. Tenenbaum, and H. C. Wolf. Detection of roads and linear structures in low-resolution aerial imagery using a multisource knowledge integration technique. *Computer Graphics and Image Processing*, 15:201–223, 1981.

[4] D. Geman and B. Jedynak. An active testing model for tracking roads in satellite images. *IEEE Trans. on PAMI*, 18:1–14, 1996.

[5] C. J. Geyer and J. Møller. Simulation and likelihood inference for spatial point process. *Scandinavian Journal of Statistics, Series B*, 21:359–373, 1994.

[6] P.J. Green. Reversible jump Markov chain Monte-Carlo computation and bayesian model determination. *Biometrika*, (57):97–109, 1995.

[7] C. Hivernat, X. Descombes, S. Pandriamasy, and J. Zerubia. Mise en correspondance d'un couple de réseaux linéiques : application à l'analyse et au recalage de réseaux routiers extraits d'un couple carte/image spot. *Traitement du signal*, 17(1):21–32, 2000.

[8] M. Imberty and X. Descombes. Simulation de processus objets : Etude de faisabilité pour une application à la segmentation d'images. Research Report (Rapport de Recherche, in French) 3881, INRIA, February 2000.

[9] H. Mayer, I. Laptev, H. Mayer, A. Baumgartner, and C. Steger. Automatic road extraction based on multi-scale modeling, context and snakes. *International Archives of Photogrammetry and Remote Sensing*, 32:106–113, 1997.

[10] N. Merlet and J. Zerubia. New prospects in line detection by dynamic programming. *IEEE Trans. on PAMI*, 18(4):426–431, 1996.

[11] M. Metropolis, A. W. Rosenbluth, A. H. Teller, and E. Teller. Equation of state calculations by fast computing machines. *Journal of Chemical Physics*, 21:1087–1092, 1953.

[12] W. M. Neuenschwander, P. Fua, L. Iverson, G. Székely, and O. Kubler. Ziplock snakes. *International Journal of Computer Vision*, 25(3):191–201, 1997.

[13] M. Ortner. Extraction de caricatures de bâtiments sur des modèles numériques d'élévation. Master thesis (Rapport de DEA, in French), INRIA, August 2001. `http://www-sop.inria.fr/ariana/personnel/Mathias.Ortner/rapport_DEA_ortner.ps.gz`.

[14] C. Preston. Spatial birth and death processes. *Bulletin of the International Statistical Institute*, 46(2):371–391, 1976.

[15] G. Rellier, X. Descombes, and J. Zerubia. Local registration and deformation of a road cartographic database on a SPOT satellite image. Research Report 3939, INRIA, May 2000.

[16] B. D. Ripley. Modelling spatial patterns. *Journal of the Royal Statistical Institute, Series B*, 39:172–212, 1977.

[17] C. Robert and G. Casella. *Monte Carlo Statistical Methods*, chapter 8. Springer-Verlag, 1999.

[18] H. Rue and A. R. Syverseen. Bayesian object recognition with Baddeley's delta loss. *Adv. Appl. Prob*, 30:64–84, 1998.

[19] D. Ruelle. Superstable interactions in classical statistical mechanics. *Communication in Mathematical Physics*, 18:127–159, 1970.

[20] J-P. Sampère. Evaluation de l'utilisation de données supermode SPOT5 pour la mise à jour de BD IGN. *Bulletin de la S.F.T.P.*, (164/165):96–105, 2001-4/2002-1.

[21] R. Stoica. Processus ponctuels pour l'extraction des réseaux linéiques dans les images satellitaires et aériennes. PhD thesis (Thèse, in French), University of Nice Sophia-Antiopolis, February 2001.

[22] M.N.M. van Lieshout. Stochastic annealing for nearest-neighbour point processes with application to object recognition. Research Report BS-R9306, CWI, 1993.

[23] M.N.M. van Lieshout and R.S. Stoica. The Candy model revisted : Markov properties and inference. Research Report PNA - R0115, CWI, 2001.

[24] A. Zlotnick and P. Carnine. Finding road seeds in aerial images. *Computer Vision, Graphics, and Image Processing*, 57:243–260, 1993.

Unité de recherche INRIA Sophia Antipolis
2004, route des Lucioles - BP 93 - 06902 Sophia Antipolis Cedex (France)

Unité de recherche INRIA Lorraine : LORIA, Technopôle de Nancy-Brabois - Campus scientifique
615, rue du Jardin Botanique - BP 101 - 54602 Villers-lès-Nancy Cedex (France)
Unité de recherche INRIA Rennes : IRISA, Campus universitaire de Beaulieu - 35042 Rennes Cedex (France)
Unité de recherche INRIA Rhône-Alpes : 655, avenue de l'Europe - 38330 Montbonnot-St-Martin (France)
Unité de recherche INRIA Rocquencourt : Domaine de Voluceau - Rocquencourt - BP 105 - 78153 Le Chesnay Cedex (France)

Éditeur
INRIA - Domaine de Voluceau - Rocquencourt, BP 105 - 78153 Le Chesnay Cedex (France)
http://www.inria.fr
ISSN 0249-6399